Proc. 23rd Winter Workshop on Nuclear Dynamics (2007) 000–000

23rd Winter Workshop on Nuclear Dynamics
Big Sky, Montana, USA
February 11–18, 2007

Mapping out the Jet correlation landscape: Jet quenching and Medium response

Jiangyong Jia[1] for the PHENIX Collaboration

[1] Chemistry Department, Stony Brook University

Abstract. A selected set of di-hadron correlation results from PHENIX are discussed. These results provide evidences for four distinct contributions concentrated at various $\Delta\phi$ ranges. The p_T, particle species and energy dependence of these contributions reflect detailed interplay between jet quenching and response of the partonic matter to the lost energy.

Keywords: Quark Gluon Plasma, Jet Quenching, Medium Response
PACS: 25.75.NQ, 25.75.-q

1. Introduction

High p_T partons are valuable probes of the high energy density matter created at the Relativistic Heavy-Ion Collider (RHIC). These partons are expected to loose a large fraction of their energy traversing the dense matter. This energy loss picture was quite successful [1] in reproducing the experimental observed [2, 3] suppression of single hadron and di-hadron yield at high p_T.

The high p_T hadron yield are normally calculated as,

$$\text{Yield} \propto \int_{\vec{\mathbf{r}},\widehat{\mathrm{p_T}},\Delta\mathrm{E},\mathrm{z}} \mathrm{G}(\vec{\mathbf{r}}) \otimes \mathrm{f}(\widehat{\mathrm{p_T}}) \otimes \mathrm{P}(\Delta\mathrm{E},\phi,\vec{\mathbf{r}}) \otimes \mathrm{D_{vac}}(\mathrm{z},\widehat{\mathrm{p_T}}-\Delta\mathrm{E}) \qquad (1)$$

Where $G(\vec{\mathbf{r}})$ is the nuclear overlap geometry via Glauber model, $f(\widehat{p_T})$ is the parton p_T spectra after hard-scattering, $P(\Delta E,\phi,\vec{\mathbf{r}})$ represents the position and emission angle dependent probability distribution of total energy loss, and $D_{vac}(z,\widehat{p_T}-\Delta E)$ is the fragmentation function of the parton in vacuum with energy of $\widehat{p_T}-\Delta E$. In principle, dynamics of the parton-medium interaction are all embedded $P(\Delta E,\vec{\mathbf{r}})$. However, the experimentally observed large suppression, up to factor of 4-5 in central Au+Au collisions, implies that the medium is extremely opaque and most of the detected high p_T hadrons comes from surface region of the medium, so called "surface bias" [4] (i.e. $\widehat{p_T}-\Delta E\sim 0$ other than the surface). This bias is exacerbated by the steeply-falling-ness of the parton spectra $f(\widehat{p_T})$, leading to a situation where the dependence of high p_T yield on $P(\Delta E,\vec{\mathbf{r}})$ is reduced to an overall nor-

malization factor that is fixed by the experimentally measured R_{AA}, which varies with energy loss models. But single hadron yield can't constrain the shape of $P'(\Delta E) = \int d\phi d\vec{\mathbf{r}} P(\Delta E, \phi, \vec{\mathbf{r}})$, hence the dynamics of energy loss models, very well (the fragility [5]).

To regain sensitivity to the energy loss mechanisms, one inevitably need to study the distribution of the energy lost by the partons via two- or multi-particle correlations. For intermediate p_T charged hadron pairs, the away-side jet was observed to peak at $\Delta\phi \sim \pi \pm 1.1$ [6, 7], suggesting that the energy lost by high p_T partons is transported to lower p_T hadrons at angles away from $\Delta\phi \sim \pi$. The proposed mechanisms for such energy transport include medium deflection of hard [8] or shower partons [9], large-angle gluon radiation [10, 11], Cherenkov gluon radiation [12], and "Mach Shock" medium excitations [13].

In this proceeding, we discuss some aspects of the di-hadron correlation results from PHENIX, with an eye to constrain the possible energy loss mechanism as well the response of the partonic matter to the energy loss.

2. Away-side p_T scan: Medium-induced component and Punch-through component

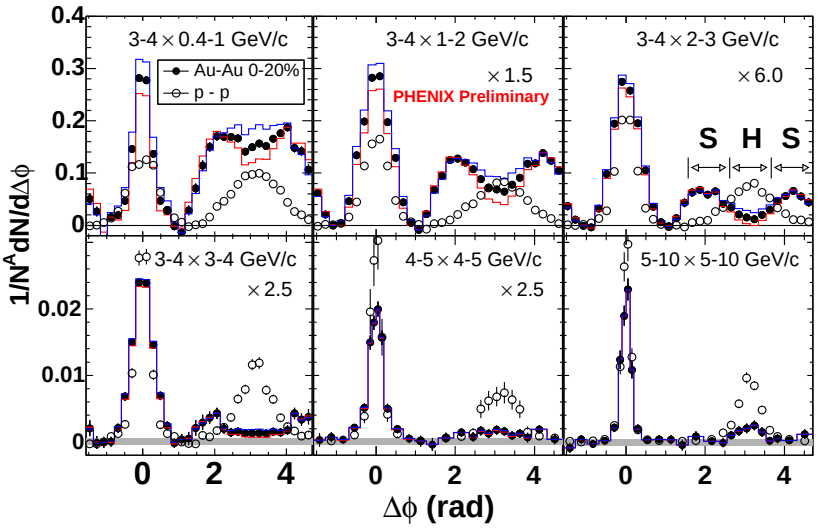

Fig. 1. Per-trigger yield vs. $\Delta\phi$ for various trigger and partner p_T ($p_T^A \otimes p_T^B$) in p+p and 0-20% Au+Au collisions. The Data in some panels are scaled as indicated. Solid lines (shaded bands) indicate elliptic flow (ZYAM method) uncertainties. Arrows in Fig. 1c depict the "Head Region" (**H**) and the "Shoulder Region" (**S**).

Fig.1 shows the per-trigger yield distributions for $p + p$ and central Au+Au

collisions for various combinations of trigger and partner p_T ranges ($p_T^A \otimes p_T^B$). The $p+p$ data show essentially Gaussian away-side peaks centered at $\Delta\phi \sim \pi$ for all p_T^A and p_T^B. In contrast, the Au+Au data show a shape modifications that is dependent on p_T^A and p_T^B. For a fixed value of p_T^A, Figs. 1a - 1d show that the away side evolves from a broad peak to a local minimum at $\Delta\phi \sim \pi$ with side-peaks at $\Delta\phi \sim \pi \pm 1.1$. The location of the side-peaks in $\Delta\phi$ is roughly constant with increasing p_T^B (Note [7] also shows that the peak location is relatively insensitive to centrality and system size). Such p_T independence is compatible with the away-side jet modification expected from "Mach Shock" [13] but disfavors models which incorporate large angle gluon radiation [10, 11], Cherenkov gluon radiation [12] or deflected jets [8, 9].

For relatively high values of $p_T^A \otimes p_T^B$ (Figs. 1e - 1f), the away-side jet shape for Au+Au gradually becomes peaked as for $p+p$, albeit suppressed. This "re-appearance" of the away-side peak seems due to a reduction of the yield centered at $\Delta\phi \sim \pi \pm 1.1$ relative to that at $\Delta\phi \sim \pi$, rather than a merging of the peaks centered at $\Delta\phi \sim \pi \pm 1.1$. This is consistent with the dominance of di-jet fragmentation at large $p_T^A \otimes p_T^B$, possibly due to jets that "punch-through" the medium [14] or those emitted tangentially to the medium's surface [15].

The evolution of the away-side jet shape with p_T (cf. Fig. 1) suggests two distinctive components at the away-side: a medium-induced component centered at $\Delta\phi \sim \pi \pm 1.1$ (Shoulder Region, SR) and a fragmentation component centered at $\Delta\phi \sim \pi$ (Head Region, HR). The away-side is dominated by the former at $p_T^{A,B} < 4$ GeV/c, and by the later at higher p_T. However, we notice that HR can be strongly contaminated by feed in from the SR, especially at low $p_T^{A,B}$.

3. Chemistry of the Medium-induced component

To elucidate the underlying physics of the medium-induced component, we focus on the intermediate p_T where the SR is dominating, and study the particle composition of the yield in SR. Fig.2a show a comparison of the partner meson and baryon yield in 1.6-2.0 GeV/c associated with charged hadron triggers in 2.5-4 GeV/c. Interestingly, both partner mesons and baryons show very similar concave shape, suggesting a similar physics origin.

Fig.2b shows ratios of the away-side parter baryon yield and meson yield as function of partner p_T for several centrality bins. The ratios grow steadily with increasing partner p_T, and the increase is strongest in most central Au+Au collisions. We notice that the baryon/meson ratio in the away-side jet is close but slightly lower than that obtained for inclusive hadrons (dashed lines). These results strongly disfavors large angle hard radiation [10, 11] or simple bending jet [8, 9] models, where the partons are radiated off-center or deflected by the medium followed by fragmentation in vacuum. In "Mach Shock" scenarios, the energy lost by propagating partons is absorbed by the medium and converted into collective conic flow. No new partons are produced, instead the fluid elements are boosted in the

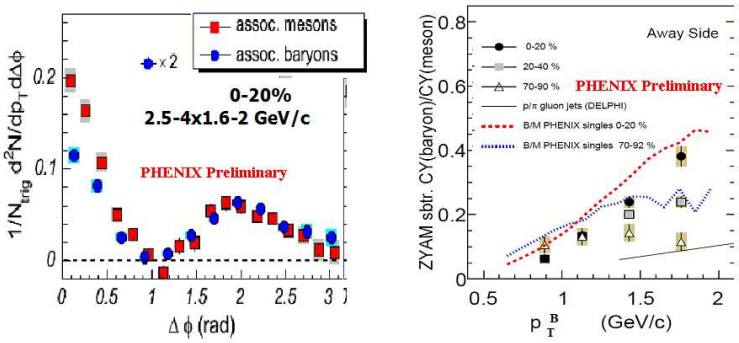

Fig. 2. a) The associated partner meson and baryon $\Delta\phi$ distribution. b) Ratio of partner baryon to meson at the away-side vs. partner p_T for 0-20%, 20-40% and 70-90% centrality bin. For both panels, triggers are charged hadrons in $2.5 < p_T < 4.0$ GeV/c.

Mach angle [16] and then fragments via recombination. This would naturally lead to a centrality dependent baryon/meson ratio similar to that for inclusive hadrons.

4. Energy dependence of the Medium-induced component

Further insights on the physics of SR can be obtained by the studying its $\sqrt{s}$ dependence. In particular, it is interesting to see whether the two-component picture applies at much lower collision energy. The results from the three collision energies ($\sqrt{s_{NN}}$ = 200, 62.4, and 17.3 GeV) for $1 < p_T^B < 2.5 < p_T^A < 4$ GeV/c are shown side by side in 3. The distribution becomes less concave at lower $\sqrt{s}$. At SPS energy ($\sqrt{s}$ = 17.2 GeV from CERES [17]), the away-side looks almost flat, which might imply a reduced medium-induced component at lower $\sqrt{s}$. But the overall jet shape is still strongly modified.

For $\sqrt{s_{NN}}$ = 62.4 GeV data, only the jet pair fraction is shown. However for both 200 GeV and 17.2 GeV data, the absolute efficiency corrected jet yield are shown, which allow a quantitative comparison. The η coverage of CERES Time Projection Chamber corresponds to 0.1-0.7 in CM frame at $\sqrt{s_{NN}}$ = 17.3 GeV. Its rapidity window of 0.6 is close to 0.7 for PHENIX, the corresponding jet yield can be compared directly with that at 200 GeV after corrected by 0.7/0.6 = 1.17. From Fig.3, the maximum and minimum value are 0.17 and 0.07 for 0-5% Au+Au collisions at 200 GeV. They are 0.08 and 0.07 for 0-5% Pb+Pb collisions at 17.3 GeV after the acceptance correlation. Thus the amplitude of the SR in CERES is about factor 2 lower than PHENIX value, whereas the yield at the HR is surprisingly close to the PHENIX value. The former possibly suggests a weaker medium effect at SPS, while the latter probably is more complicated to interpret. On the one

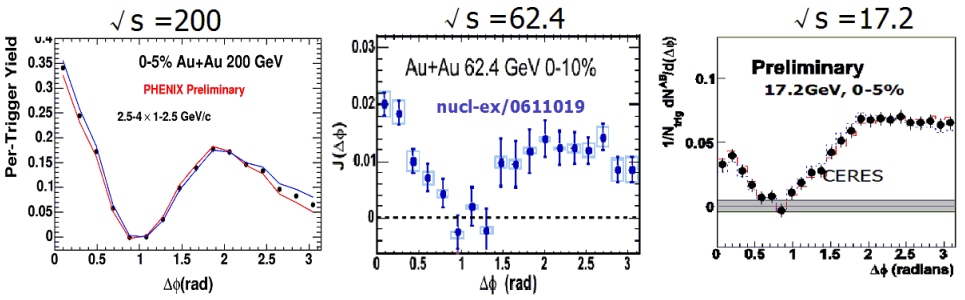

Fig. 3. a) Per-trigger yield in central Au+Au collisions at $\sqrt{s_{\rm NN}} = 200$ GeV from PHENIX. b) The extract jet function at $\sqrt{s_{\rm NN}} = 62.4$ GeV from PHENIX. c) Per-trigger yield at $\sqrt{s_{\rm NN}} = 17.3$ GeV from CERES [17].

hand one expect a higher jet multiplicity at RHIC than at SPS, due to a smaller $\langle z \rangle$. On the other hand, the jet quenching is stronger at RHIC than that in SPS. Maybe the fact that the similar HR yield at the two energies is just coincidence. Further detailed study of the $\sqrt{s}$ dependence of the punch-through and medium-induced components can provide crucial constrains on the turn on of jet quenching and medium response.

5. Near-side p_T scan: Jet fragmentation and the Ridge

Fig.1 suggests that, relative to p+p, the near-side jet is also modified in central Au+Au collisions. Fig.4 shows the near-side jet width as function of centrality for an intermediated p_T bin, $2.5-4 \otimes 1-2$ GeV/c, and a high p_T bin, $5-10 \otimes 2.5-4$ GeV/c. The former shows a significant broadening of the jet width in central Au+Au collisions, while the latter shows essentially unmodified jet width. These features suggest that the modification on the near-side jet is limited to intermediate p_T.

The modification of the jet multiplicity can be quantified by $I_{\rm AA}$, the ratio of per-trigger yield in Au+Au to that in $p+p$ for $|\Delta\phi| < \pi/3$:

$$I_{\rm AA} = \int_{|\Delta\phi|<\pi/3} d\Delta\phi Y_{\rm jet}^{\rm Au+Au} \Big/ \int_{|\Delta\phi|<\pi/3} d\Delta\phi Y_{\rm jet}^{p+p} \qquad (2)$$

Fig.5 shows near-side $I_{\rm AA}$ as function of partner p_T at for three trigger p_T bins. We see an enhancement at low partner p_T, which diminishes toward high partner p_T. With increasing trigger p_T, the $I_{\rm AA}$ distributions become flatter in partner p_T. The near-side enhancement has been observed by the STAR collaboration [18] and was shown to be due to a long range $\Delta\eta$ correlation which extends out in $\Delta\eta$ up to ± 2 and sits on top of the regular jet component. The decrease of the enhancement with increasing trigger p_T implies that the ridge component is softer than the jet

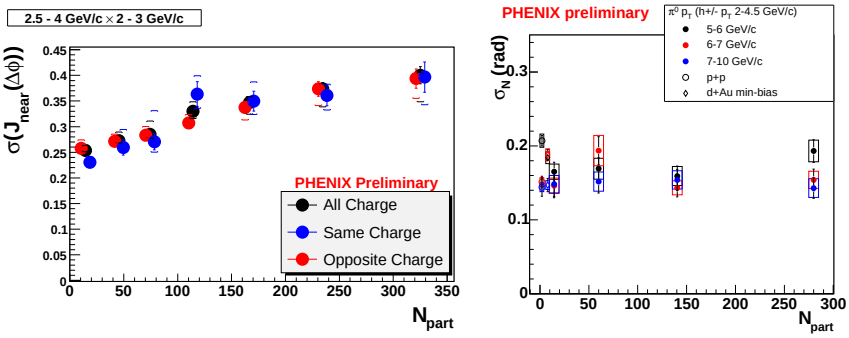

Fig. 4. Centrality dependence of the near side gauss width in 200 GeV Au+Au collisions at intermediate p_T of $2.5-4\times2-3$ GeV/c (Left) and at various high p_T bins above 5 GeV/c (Right).

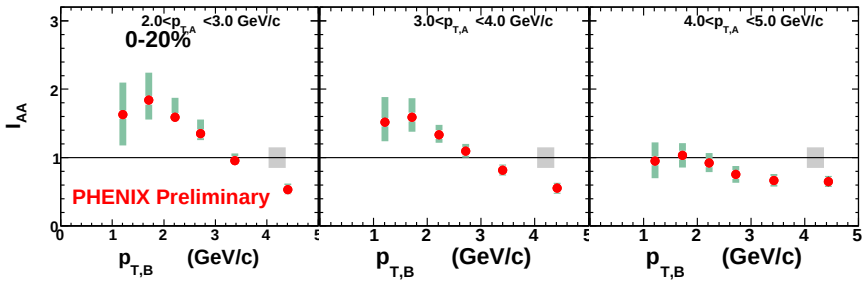

Fig. 5. Near-side $I_{\rm AA}$ (in $|\Delta\phi|<\pi/3$) for three trigger p_T bins in 0-20% central Au+Au collisions at 200 GeV.

component. Results on both the near-side widths and yields suggest that the p_T range where the ridge yield is important is limited to $p_T^A, p_T^B < 4$ GeV/c. This range is very similar to that for the away-side enhancement seen in SR (i.e. Fig.1).

Due to its limited η acceptance, PHENIX so far haven't be able to directly observe the ridge signature. But its study of near-side jet shape and yield in broad p_T range can still provide valuable constraints on the properties of the ridge.

6. Discussion

Our investigation of jet-induced pairs suggests that they are consistent of four distinct components concentrated at various $\Delta\phi$ regions with their characteristically distinct dependence on p_T, PID, $\sqrt{s}$ etc: 1) A hard component around $\Delta\phi\sim0$ that is consistent with fragmentation of jet emitted from surface ("Surface"; 2) A

soft and broad component at the near-side ("Ridge"); 3) A hard component around $\Delta\phi \sim \pi$ consistent with fragmentation of punch-through jet ("Head"); and 4) a soft component centered at $|\Delta\phi - \pi| \sim 1.1$ ("Shoulder"). The hard components ("Surface" and "Head") are sensitive to the quenching power of the medium: The hard component at the near-side shows little modification, whereas the hard component at the away-side are suppressed by factor of 5 in central Au+Au collisions. The soft components ("Ridge" and "Shoulder") reflect the response of the medium to the jets, appearing as distortions of the shape and enhancements of the yield. They are shown to be important at $p_T^{A,B} < 4$ GeV/c and have a particle composition that is closer to the bulk medium. The non-trivial evolutions of the near- and away-side shape/yield with p_T and $\sqrt{s}$ probably reflects the detailed interplay between the soft and hard components.

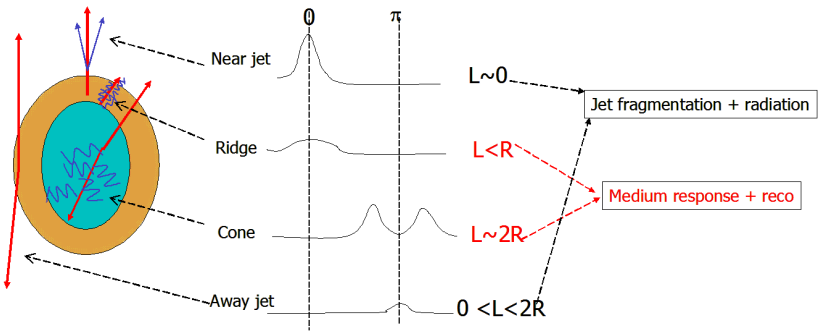

Fig. 6. A sketch of the four different di-jet events (left), and the corresponding four $\Delta\phi$ distribution (middle) and typical path lengths (rights).

These four components, though initiated by the same original back-to-back hard partons, may have very different geometrical distribution and dynamical processes in the medium as illustrated in Fig.6 (see also [19]). In a simple jet absorption picture where a very opaque medium is assumed [4], the near-side hard component is emitted from close to the surface, $\langle L \rangle \sim 0$; the near-side "Ridge" reflects medium response to the near-side jet, thus could be initialed by the hard partons at a small distance from the surface: $\langle L \rangle < R$ (R is the average radius of the medium); the away-side "Shoulder" could be initiated by jet that span a large path length, $\langle L \rangle > R$; the path length for away-side hard component can vary dramatically depends whether it is tangential emission or punch-through, $0 < \langle L \rangle < 2R$. Note that the basic $\Delta\phi$ distributions, i.e Fig.1, are obtained statistically. They reflect the combined distribution of many jet pairs from many events. However, the average number of jet pairs for any given $p_T^A \otimes p_T^B$ is typically much less than 1, thus the jet pairs in given event typically come only from one of the four components. The overall distribution can be regarded as the sum of the four types of events shown in left column of Fig.6.

One important next step in correlation analysis is to quantitatively separate the four components, and to study their properties in detail. To fully understand the medium response, one need to understand whether the near-side "Ridge" and away-side "Shoulder" are of the same origin or not. The three particle correlation, as well as detailed mapping of the p_T, PID, charge and $\sqrt{s}$ dependence of two particle correlation would be very helpful in this regard. In additional, one can dial the path length by triggering on two high p_T hadrons and correlate with the third soft hadron, the "displaced" peak might be seen on both the near- and away-side [14]. However this is possible only if the high p_T hadrons have a significant punch-through component and the medium can not be very opaque. On the other hand, the high p_T di-hadron and gamma-jet correlation remains to be a good tomographic tool since it is less affected by the surface bias than the single spectra measurements [20, 21]. Both the centrality and reaction plane dependence of the jet correlation at high p_T would be very helpful in constraining various jet quenching models.

References

1. M. Gyulassy, I. Vitev, X. N. Wang and B. W. Zhang, nucl-th/0302077; A. Kovner and U. A. Wiedemann, hep-ph/0304151.
2. S. S. Adler *et al.* Phys. Rev. C **69**, 034910 (2004)
3. J. Adams *et al.* Phys. Rev. Lett. **97**, 162301 (2006)
4. A. Drees, H. Feng and J. Jia, Phys. Rev. C **71**, 034909 (2005)
5. K. J. Eskola *et al.*, Nucl. Phys. A **747**, 511 (2005) [arXiv:hep-ph/0406319].
6. S. S. Adler *et al.* Phys. Rev. Lett. **97**, 052301 (2006)
7. A. Adare *et al.* nucl-ex/0611019.
8. C. Chiu and R. Hwa, Phys. Rev. C **74**, 064909 (2006)
9. N. Armesto, C. A. Salgado and U. A. Wiedemann, Phys. Rev. Lett. **93**, 242301 (2004)
10. I. Vitev, Phys. Lett. B **630**, 78 (2005)
11. A. D. Polosa and C. A. Salgado, Phys. Rev. C **75**, 041901 (2007)
12. I. M. Dremin, JETP Lett. **30** (1979) 140; V. Koch, A. Majumder and X. N. Wang, Phys. Rev. Lett. **96**, 172302 (2006)
13. J. Casalderrey-Solana, E. V. Shuryak and D. Teaney, hep-ph/0602183.
14. T. Renk and K. J. Eskola, hep-ph/0610059.
15. C. Loizides, Eur. Phys. J. C **49**, 339 (2007)
16. T. Renk and J. Ruppert, Phys. Rev. C **73**, 011901 (2006)
17. M. Ploskon, Nucl. Phys. A **783**, 527 (2007)
18. J. Adams *et al.* Phys. Rev. Lett. **95**, 152301 (2005)
19. T. Renk and J. Ruppert, arXiv:hep-ph/0701154.
20. H. Zhang, J. F. Owens, E. Wang and X. N. Wang, arXiv:nucl-th/0701045.
21. T. Renk, Phys. Rev. C **74**, 034906 (2006) [arXiv:hep-ph/0607166].